Study of heat of adsorption across the capillary condensation in cylindrical pores

Yao Wang, D.D. Do*, D. Nicholson

School of Chemical Engineering, University of Queensland, St. Lucia, Qld 4072, Australia

ARTICLE INFO

ABSTRACT

We have investigated the isosteric heat of argon adsorption in MCM-41 and carbon nanotubes using grand canonical Monte Carlo (GCMC) simulation, and find that the isosteric heat during the capillary condensation is practically constant irrespective of temperature, pore-curvature, and surface strength. We also studied the microscopic behavior during capillary condensation by analyzing the histogram of the number of particles, the local number fluctuation and the layer compressibility. The histograms exhibit increasingly broader peaks close to condensation which subdivide into two separate peaks, indicating the relative probability of two co-existing states. Local number fluctuation allows us to identify the boundary between the adsorbed phase and the gas phase inside the pore. The layer compressibility can be used to identify the states of the adsorbate in each layer within the adsorbed phase. Finally we propose a simple model for the heterogeneous surface of MCM-41 to simulate the effects of surface heterogeneity on the isosteric heat. This model is able to describe the experimental isosteric heat of argon adsorption at 87.3 K in MCM-41.

1. Introduction

Capillary condensation is an important topic in adsorption engineering, particularly in its application to the characterization of mesoporous materials for surface area, pore size distribution, and porosity [1]. Both experimental and computational research has been pursued to understand this phenomenon, especially the hysteresis loop shape and size, the critical hysteresis temperature, the pore critical temperature and the pressures at which the condensation and evaporation occur.

Experimental and theoretical studies of capillary condensation have been reviewed in the literature [1,2]. Just to highlight a few examples, Burgess et al. [3] studied experimentally the decrease of hysteresis loop size with temperature and drew attention to the existence of a hysteresis critical temperature; de Boer discussed the shape of hysteresis loop [4] and this was later further elaborated in later work [1,2]. Thommes and Findenegg [5] observed the shift in the hysteresis critical point with pore width; Morishige and Shikimi [6] measured the slope of the isotherm during condensation to estimate the pore critical temperature. There are several simulation studies of the microscopic details of the capillary condensation. Peterson et al. [7] used NLDFT to study the effects of pore radius, pressure, temperature and surface strength on the behavior of capillary condensation. Neimark et al. [8] identified different sorption regimes depending on the pore size and temperature by using MC simulation and NLDFT. Coasne et al. [9,10], also using GCMC, proposed a general rule relating the critical capillary temperature to the bulk system properties. They also found that the pore length and the surface disorder strongly influence the shape and size of the hysteresis loop. Gelb [11], using GCMC simulation, found that hysteresis is absent in closed pores.

Although many studies on capillary condensation have been reported, very few have placed emphasis on the behavior of the isosteric heat. Zhuo et al. studied isosteric heats for the adsorption of pure and mixed carbon dioxide and nitrogen adsorption on MCM-41 by simulation to show that CO_2 is more preferentially adsorbed in MCM-41 [12]; Neimark et al. [13] calculated isosteric heats of argon adsorption from the experimental data. Siperstein et al. [14,15] compared the isosteric heats of argon and krypton adsorption on smooth and heterogeneous surfaces. Maddox and Gubbins [16] studied the isosteric heat of argon and nitrogen adsorption on smooth double buckytubes (carbon nanotubes) and MCM-41 using GCMC simulation. Also using GCMC simulation, Coasne et al. [17,18] found that surface disorder in a cylindrical pore overestimates the experimental isosteric heat and suggested that the isosteric heat cannot be used to gain information of the pore's morphological defects, since the contributions to the heat curves from different pore sizes and different constriction conditions are not distinct. Coasne et al. [19] also used isosteric heat to study the effects of different potential models for nitrogen adsorption in a cylindrical pore and found that the two site model for nitrogen is more sensitive to the surface heterogeneity compared to the one site model. Bhattacharya et al. [20] studied adsorption of argon in SBA-15 using an atomistic model for the adsorbent; their simula-

* Corresponding author. Tel.: +61 7 3365 4154; fax: +61 7 3365 2789.
E-mail addresses: d.d.do@uq.edu.au, duongd@cheque.uq.edu.au (D.D. Do).

Table 1
Parameters for LJ potential.

	$\rho_s \varepsilon_{sf}/k_B$ (K/nm^2)	σ_{sf} (nm)
Graphitized carbon	2212.4	0.340
MCM-41	2620.0	0.300

tion data show constant heat of adsorption during the condensation process. Similarly Olivier [21] compared the experimental results of argon adsorption on mesoporous silica with those from density functional theory calculations and found that the isosteric heat during the condensation process is almost constant. Pellenq and Levitz [22] reported the isosteric heat for argon, krypton and xenon adsorption on a heterogeneous surface of a reconstructed porous vycor glass by GCMC and pointed out that the heat reached a plateau at the onset of capillary condensation.

In this paper, we use GCMC simulation to study condensation by examining various properties such as local density, local number fluctuation and local compressibility to analyze the behavior of isosteric heat. We use graphitized carbon nanotubes and MCM-41 cylindrical pores as the model solid substrates, and argon as the model adsorbate.

2. Theory

2.1. GCMC simulation method

Adsorption equilibrium was studied using Grand Canonical Monte Carlo simulation (GCMC). In the simulations, we used 20,000 cycles for the equilibrium and sampling stages. Each cycle consisted of one thousand displacement moves and attempts to either insert or delete with equal probability. The box lengths were set to twice the pore radius and periodic boundary conditions applied at the two boundaries in the axial direction to simulate a cylinder of infinite extent. The cut-off radius was set to half the box length. The displacement step length was initially set at half the box length in the axial direction, and then adjusted during the equilibration stage to achieve an acceptance ratio of the displacement move of between 20 and 25%. We studied the adsorption of argon on cylindrical pores of size of 3.6 nm, 4.4 nm and 5.1 nm at 77, 87.3 and 99 K.

2.2. Fluid–fluid and solid–fluid interaction

The Lennard–Jones (LJ) model was used to calculate the fluid–fluid interaction potential. The LJ parameters for argon are $\varepsilon_{ff} = 119.8$ K and $\sigma_{ff} = 0.3405$ nm. We consider two pore surfaces: graphitic and MCM-41 cylindrical surfaces. Assuming the surface is homogeneous and has a constant surface density, ρ_S the solid–fluid potential energy can be calculated from the following equation [23], previously used by several workers [13,24,25]

$$U_{SF} = 4\pi^2 \rho_S \sigma_{sf}^2 \varepsilon_{sf}(I_6 - I_3) \tag{1a}$$

$$I_6 = \frac{63}{128}\left(\frac{\sigma_{sf}}{R}\right)^{10}\left[1 - \left(\frac{r}{R}\right)^2\right]^{-10} \cdot F\left[-\frac{9}{2}; -\frac{9}{2}; 1; \left(\frac{r}{R}\right)^2\right]; \tag{1b}$$

$$I_3 = \frac{3}{4}\left(\frac{\sigma_{sf}}{R}\right)^4\left[1 - \left(\frac{r}{R}\right)^2\right]^{-4} \cdot F\left[-\frac{3}{2}; -\frac{3}{2}; 1; \left(\frac{r}{R}\right)^2\right] \tag{1c}$$

where ρ_S is the surface density, r is the normal distance from the pore wall surface to the argon particle, R is the radius of the cylindrical pore and $F[a;b;c;d]$ is a hypergeometric function. The cross solid–fluid parameters are calculated from the Lorentz–Berthelot rule. For the graphitic and silica (MCM-41) surfaces, the relevant cross molecular parameters are given in Table 1. The cross well depth parameter, $\rho_s \varepsilon_{sf}$ of MCM-41 is larger than that of the
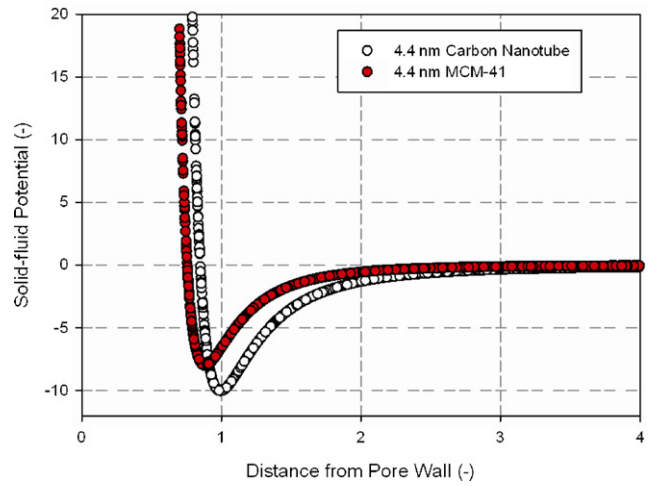
Fig. 1. Solid–fluid potential of 4.4 nm MCM-41 and 4.4 nm carbon nanotube.

graphite surface, giving a false impression that the MCM-41 surface is stronger than the graphitic surface. In fact, the strength of a surface does not depend on just $\rho_s \varepsilon_{sf}$ but rather $\rho_s \varepsilon_{sf} \sigma_{sf}^2$. Since the parameter σ_{sf} of the graphitic surface is greater than that of the silica surface, $(\sigma_{sf}^2)_{Graphite}/(\sigma_{sf}^2)_{Silica} = 2.26$, the product $\rho_s \varepsilon_{sf} \sigma_{sf}^2$ of the
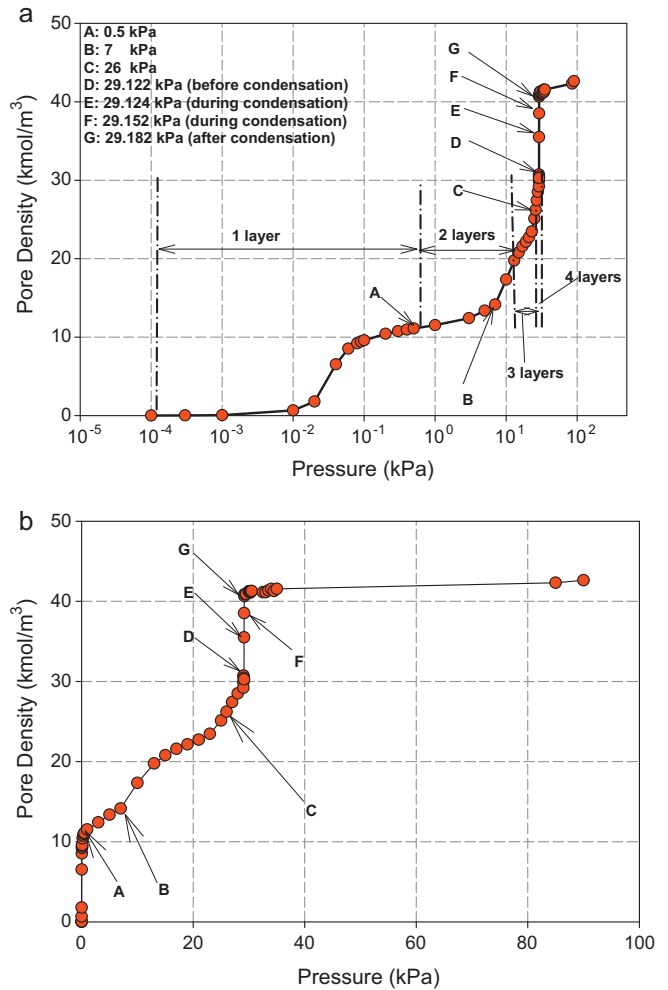
Fig. 2. Isotherm for the adsorption of argon in a 4.4 nm carbon nanotube at 87.3K, (a) semi-log scale and (b) linear scale. The vertical line D, E, F, G shows the location of the spontaneous capillary condensation.